J Therm Anal Calorim (2011) 104:1055–1062
DOI 10.1007/s10973-010-1201-2

Thermal destruction of rice hull in air and nitrogen

A systematic study

Xue-Gang Chen · Shuang-Shuang Lv · Ping-Ping Zhang · Lu Zhang · Ying Ye

Received: 9 October 2010 / Accepted: 16 November 2010 / Published online: 8 December 2010

Abstract In this study, we ashed rice hull in air and nitrogen, respectively, and systematically investigated the effects of ashing temperature and atmosphere on the structures, morphologies, and pore characteristics of rice hull ash (RHA). All RHA samples are amorphous materials with porous structures. IR spectra revealed that RHA that ashed in air (WRHA) exhibit more polar groups on the surface than that of ashed in nitrogen (BRHA). The silica and carbon contents, BET surface area, and pore volume of BRHA increase with ashing temperature. When ashed in air, however, the silica content of WRHA increases and carbon content decreases with temperature. The BET surface area and pore volume of WRHA increase with temperature firstly and decline subsequently due to the closure of pores. Compared with WRHA, BRHA shows higher surface areas, micropore volumes, carbon contents, and lower mesopore fractions and silica contents. This study provides essential information for choosing a suitable thermal treatment of rice hull for a given adsorbate.

Keywords Rice hull · Thermal degradation · Air or nitrogen atmosphere · Rice husks ash · Pore structure · Adsorbent

X.-G. Chen · L. Zhang · Y. Ye (✉)
Department of Ocean Science and Engineering, Zhejiang University, Hangzhou 310028, People's Republic of China
e-mail: chenxg83@gmail.com

S.-S. Lv
Department of Nonmetallic Research, Zhejiang Institute of Geology & Mineral Resources, Hangzhou 310007, People's Republic of China

P.-P. Zhang
Second Institute of Oceanography, SOA, Hangzhou 310012, People's Republic of China

Introduction

Rice, sharing equal importance with wheat, is one of the major crops grown throughout the world. Rice is the principal staple food and nourishment for the world's population. Rice hull, or rice husk, is the milling byproduct of rice. About 500 million tons of rice is processed per annum all over the world which giving about 100 million tons of rice hull [1]. Because of its abrasive structure and low content of nutritious ingredients, rice hull is unsuitable for food and therefore is usually abandoned. Nowadays, rice hull in agriculture is usually burnt in open air or stacked on farmland, releasing large amounts of hazardous substances, occupying land resources, and polluting the environment. The utilization of rice hull, therefore, is essential to the environmental protection and treatment of agricultural waste.

The utilization of rice hull is concentrated on the utilization of carbon and silica that are rich in rice hull. Dry rice hull contains 70–85% of organic matters (including cellulose, lignine, hemicellulose, and so on) and the remainder mostly consists of silica. The silica distributes in crosslinking and constitutes the framework of rice hull. Due to its abundance, low cost, and special structure, rice hull is a good precursor for many functional materials. Particularly in the field of water purification, many effective adsorbents and composites such as rice hull ash (RHA) [2–4], rice hull-based activated carbon [5–7], silica [8, 9], zeolite[10, 11], and rice hull/ferrite composites [12, 13] have been prepared from rice hull. These rice hull-based materials have been applied to remove various contaminants from wastewater including heavy metal ions [14–16], dyes [17–19], phenol [20], and other inorganic or organic contaminants [21–23].

Various methods including thermal destruction [24, 25], chemical modification [6, 15, 26], and water vapor

treatment [27, 28] have been applied to prepare rice hull-based materials, among which thermal destruction is the cheapest, simplest, and most commonly used. The pyrolysis of rice hull and preparation of rice hull-based materials via thermal treatment have been studied extensively. For example, Sharma et al. [29] and Vlaev et al. [30] have investigated the pyrolysis kinetics and kinetic parameters of rice hull under isothermal and non-isothermal heating in air, nitrogen, or carbon dioxide. The pyrolysis kinetics of rice hull in different oxygen concentrations were also studied [31]. Markovska et al. [32] investigated the thermal destruction of rice hull in air and nitrogen atmosphere, and determined the effect of atmosphere on the structure and morphology of rice hull.

These studies, however, lack of systematic investigations on the effect of thermal destruction on the structure, morphology, and pore characteristics of rice hull, which are crucial to the adsorption capacity of adsorbent. The adsorption capacity is vital to the rice hull-based adsorbent and composites for water purification. Two major factors: the amount of adsorption sites associated with surface area and pore volume, and the adsorption force associated with pore size and chemical compositions, determine the adsorption capacity of adsorbent. Generally speaking, the adsorption capacity of adsorbent increases with its surface area and pore volume and decreases with pore size [33]. However, some organic pollutants such as methylene blue cannot enter into micro pore due to its large molecular size and meso pore volume will play a key role on the adsorption capacity. Therefore, it is essential to investigate the effects of ashing temperature and atmosphere on the structure, micro morphology, surface area, and pore structures of rice hull.

In this study, rice hull from Zhejiang Province, China, was ashed at 300–750 °C in air and nitrogen atmosphere, respectively. We systematically investigated the effects of ashing temperature and atmosphere on the chemical compositions, structures, morphologies, BET surface areas, and pore characteristics of RHA samples by means of XRD, FT-IR, SEM, EDS, and nitrogen adsorption analyses. RHA presents different physico-chemical and pore characteristics in different atmospheres and temperatures, which are important for choosing a suitable thermal treatment for a given adsorbate.

Materials and methods

Materials

Rice hull was obtained from Quzhou, Zhejiang province and was washed thoroughly by deionized water to remove the impurities and dried at 60 °C for 3 h before usage. The chemical compositions of rice hull are shown in Table 1.

Table 1 Chemical composition/% of rice hull

Organic substances	SiO_2	K_2O	CaO	MgO	P_2O_5	S	Cl	Others
79.6	19.02	0.70	0.28	0.14	0.13	0.06	0.04	0.03

Thermal destruction of rice hull

A certain amount of rice hull was placed in a furnace and was heated for 2 h at 300, 450, 600, and 750 °C, respectively. The heating rate was 5 °C min^{-1} for all samples. RHA samples were powdered and named A300–A750 (ashed in air, white rice hull ash, WRHA) or N300–N750 (ashed in nitrogen, black rice hull ash, BRHA), respectively, according to the ashing temperatures and atmospheres.

Characterizations

The phase purity and crystal structure of the samples were determined by a D/max 2550 X-ray diffractometer (XRD) (Rigaku, Japan) with Cu Kα radiation ($\lambda = 0.15406$ nm) at a scan rate of 0.02° s^{-1}. The operation voltage and current were maintained at 40 kV and 34 mA, respectively. Fourier transform infrared (FT-IR) spectra were scanned by a NICOLET 560 ESP FT-IR spectrometer (NICOLET, USA) in the range of 4,000–400 cm^{-1}. The surface morphologies and chemical compositions of the samples were studied by an S-4800 scanning electron microscope (SEM) and energy disperse spectroscopy (EDS) (Hitachi, Japan) at an accelerating voltage of 25.0 kV. Surface area and pore analysis of the samples were measured by nitrogen adsorption at 77 K using a Coulter OMNISORP surface area and pore analyzer. Bulk densities of RHA were determined using the following method: a 50 mL cylinder was filled to a specified volume with the samples that had been dried in a temperature-controlled oven at 80 °C overnight. The cylinder was tapped for at least 1–2 min to compact the samples, and then weighed. The bulk density was calculated as:

$$\text{Bulk density } \left(\text{g cm}^{-3}\right) = \text{Weight of dry sample(g)} / \text{Volume of packed dry sample } \left(\text{cm}^3\right)$$

Results and discussion

Chemical compositions and bulk densities of RHA

Figure 1 shows the carbon and silica contents of RHA samples, which change with ashing temperatures and atmospheres. Because the organic substances in rice hull

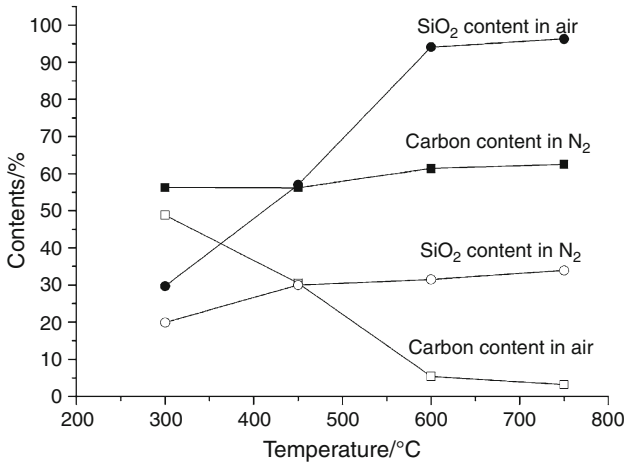

Fig. 1 Carbon and silica content of RHA samples prepared under different temperatures and atmospheres

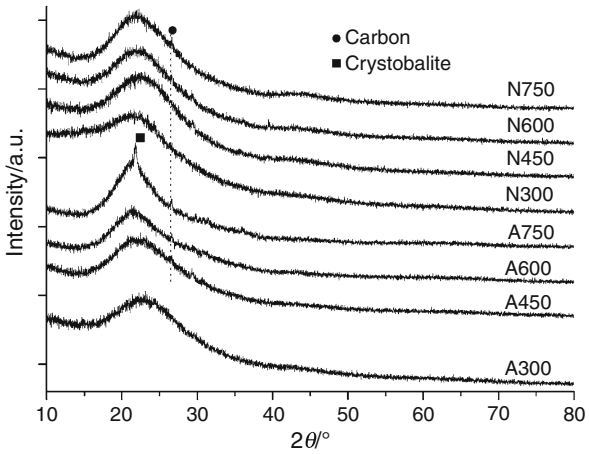

Fig. 2 XRD patterns of RHA samples prepared under different atmospheres and temperatures

such as lignin and cellulose will decompose and silica will be retained under high temperature treatment, the silica content of RHA increases with ashing temperature. For example in air atmosphere, the silica content of WRHA increases from 29.7% at 300 °C to 94.1% at 600 °C and 96.3% at 750 °C. On the contrast, the carbon content of WRHA decreases with ashing temperature, from 48.8% at 300 °C to 5.4% at 600 °C and 3.2% at 750 °C, due to the oxidation of carbon to gaseous carbon dioxide. Owing to the retention of carbon, the variations of carbon and silica contents in BRHA are much slighter than that of WRHA. The carbon content of BRHA increases from 56.3% at 300 °C to 62.5% at 750 °C (much higher than that of WRHA); and the silica content increases from 19.9% at 300 °C to 33.9% at 750 °C (much lower than that of WRHA). Generally speaking, higher carbon content will increase the pore volume especially micropore volume and physical adsorption capacity of RHA. The silica in RHA is related to chemical adsorption, where higher silica content indicates stronger chemical adsorption [34].

Bulk density values of RHA samples are generally in the same range between 0.25 and 0.33 g cm^{-3}. The bulk density of RHA that ashed in nitrogen atmosphere is slightly higher than that of RHA ashed in air due to the retention of carbon.

XRD analyses

Figure 2 shows the XRD patterns of RHA samples that prepared under different atmospheres and temperatures. All samples exhibit a diffused peak with its maximum intensity at $2\theta = 22°$, which is the characteristic of amorphous silica. The sharpness of this peak increases with ashing temperature, indicating that higher temperatures will cause higher crystallization of silica. After ashed at 750 °C in air atmosphere, the corresponding RHA sample A750 presents a sharp peak at 21.8° (marked as "filled square") which can be indexed to crystalline crystobalite. In addition, all samples except A300, N300, and N450 show a tiny peak at 26.8° which is corresponding to carbon, suggesting that the decomposition of rice hull is inadequate at 300 °C and nitrogen atmosphere will hinder the decomposition [29, 32]. The XRD analysis indicates the amorphous nature of all RHA samples that ashed in air or in nitrogen atmosphere.

FT-IR characterizations

Figure 3 shows the FT-IR patterns of WRHA and BRHA that ashed at different temperatures. Five major absorption peaks with their maximum at 3450, 1621, 1100, 800, and 467 cm^{-1} can be identified from the IR spectra. The absorption peak at 3,450 cm^{-1} can be attributed to the free and hydrogen bonded –OH groups and Si–OH group on the RHA surface, result from both the silanol groups and adsorbed water [23]. The peak at 1,621 cm^{-1} is ascribed to the stretching vibrations of C–OH groups and bending vibrations of adsorbed water. Peaks at 1100, 800, and 467 cm^{-1} are the characteristic vibration peaks of SiO_2, where 1,100 cm^{-1} is attributed to the Si–O–Si and –C–OH stretching and –OH deformation, 800 and 467 cm^{-1} indicate the presence of Si–H, as well as Si–O and Si–O–Si [35]. In addition, N300, N450, and A300 present a tiny peak at 1,712 cm^{-1}, which can be ascribed to the C–O stretching vibration of ketones, aldehydes, lactones, or carboxyl groups [36] that exist in the raw rice hull, suggesting that rice hull has not completely decomposed at 450 °C in nitrogen or 300 °C in air. The absorption peaks of WRHA are more intense than that of BRHA, indicating that WRHA exhibit more polar groups on the surface. The

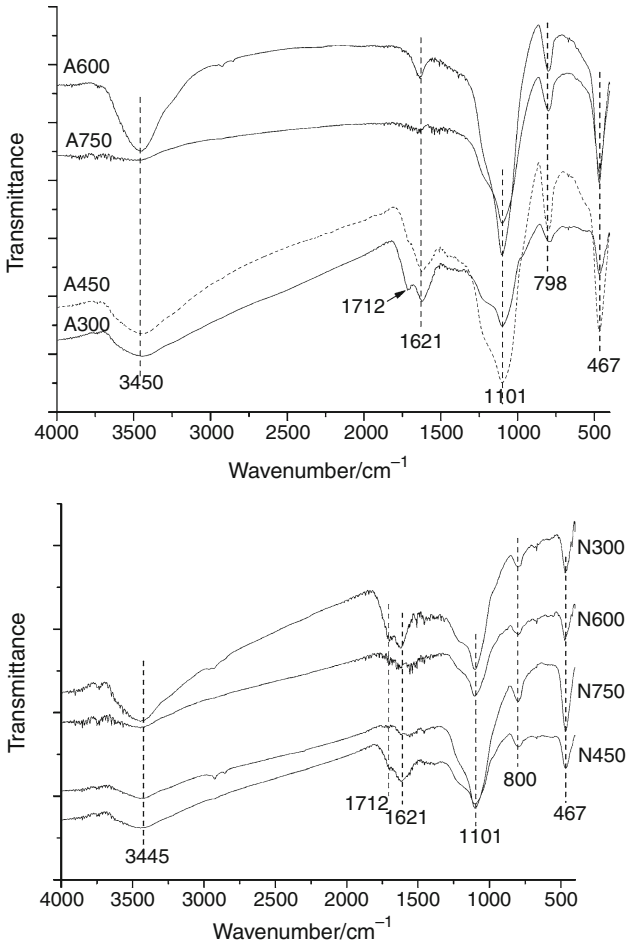

Fig. 3 FT-IR spectra of RHA samples prepared under different atmospheres and temperatures

presence of polar groups on the surface of RHA will extend the cation exchange capacity of adsorbent [37].

SEM studies

The corresponding SEM images of RHA samples are shown in Figs. 4 and 5. The surface morphologies of RHA are changing with ashing temperature and atmosphere. As we all know, higher temperature will cause more intense thermal decomposition of rice hull and nitrogen atmosphere will hinder the decomposition due to the absence of oxygen. The destruction of rice hull, therefore, will increase with ashing temperature and nitrogen atmosphere will facilitate the preservation of the original morphology of rice hull. When ashed in air, as shown in Fig. 4, the inner side of rice hull that ashed at 300 °C is smooth, indicating that the decomposition of rice hull was faint at 300 °C and the initial morphology was retained. Note that the honeycomb like pores at the cross-section of rice hull are the original pores of raw rice hull which are not induced by the decomposition of organic matters [38, 39]. The decomposition of rice hull was enhanced when the temperature was increased to 450 °C, resulted in collapsed structures in the inner side of rice hull as revealed by the SEM image. When the temperature was further increased to 600 °C, the inner side and outside parts of rice hull have decomposed intensely, square pores with edge diameters of 0.5–3 μm were formed due to the preservation of criss-crossed silica framework. The organic matter in rice hull was completely decomposed at 750 °C and the diameter of the silica framework was increased to 3–6 μm, which is the evidence of the surface melting of oxides such as K_2O and SiO_2 that induced by high temperature treatment.

When ashed in nitrogen atmosphere, as shown in Fig. 5, however, all BRHA samples that ashed at different temperatures exhibit similar morphologies. The outside part with patterned salient, the inner side part with smooth surface, and the honeycomb like pores at the cross-section of rice hull are similar in all BRHA samples. It is indicated that nitrogen atmosphere will preserve the carbon and thus the initial morphology of raw rice hull was retained.

BET surface area and pore analyses

Nitrogen adsorption and desorption analyses were conducted to investigate the surface areas and pore structures of RHA samples. Figure 6 shows the nitrogen adsorption and desorption curves of RHA samples, which present different adsorption isotherms and hysteresis loops. The adsorption and desorption curves of N300 parallels to the pressure axis with adsorption volume equals zero, indicating that N300 cannot adsorb nitrogen molecules. According to the hysteresis loops and curves, the nitrogen sorption curves of A450 fits type IV isotherm, while all the other samples show type I isotherms characterized by a nearly horizontal plateau and a "tail" near the saturation pressure. BRHA exhibits higher adsorption volumes at low pressures than that of WRHA, suggesting the more developed micropores of BRHA. The isotherm curves increase rapidly near the saturated vapor pressure, indicating the presence of mesopores, where higher mesopore volumes result in higher "tails". A600, A750, and N750 exhibit hysteresis loops at relatively high pressures, while N600, N450, A450, and A300 present low-pressure hysteresis loops. The low-pressure hysteresis is caused by the swelling of the particles which accompanies adsorption, and the swelling will be relatively minor importance when the rigidity of RHA is high [40]. Therefore, we can conclude that the rigidity of RHA is increasing with ashing temperature because A600, A750, and N750 show hysteresis loops only at high pressures. Furthermore, it is suggested that the degree of adsorbate pore blocking of BRHA is higher than that of WRHA according to the style of hysteresis loops [41], which may attributed to the higher micropore fractions of BRHA.

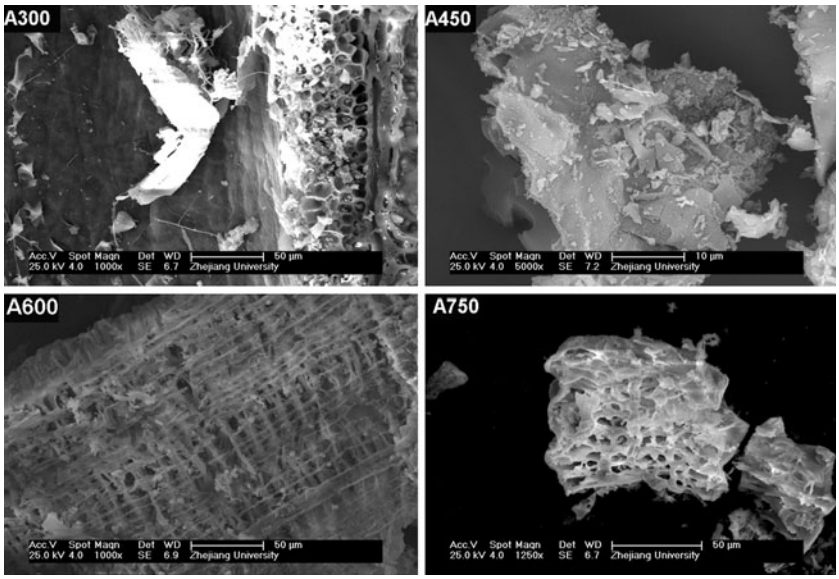

Fig. 4 SEM images of WRHA samples that ashed at different temperatures

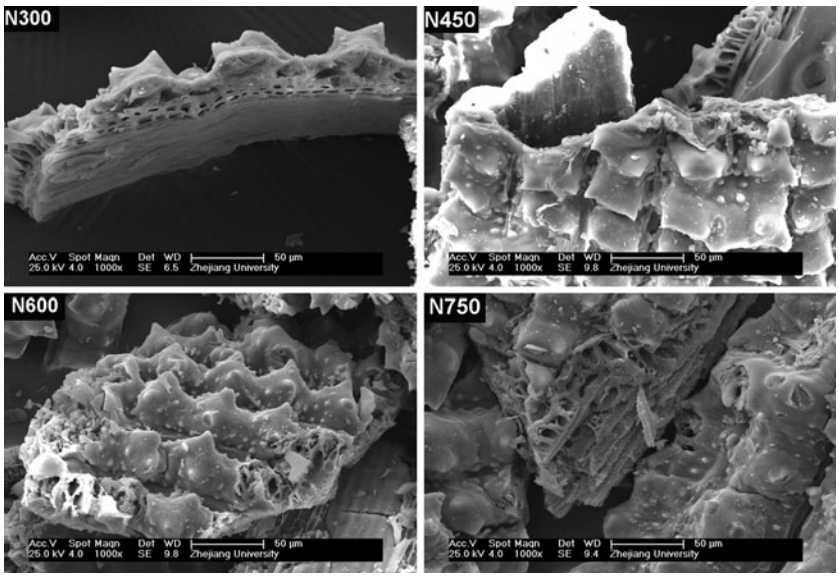

Fig. 5 SEM images of BRHA samples that ashed at different temperatures

Table 2 shows the BET surface area of RHA samples derived from the nitrogen adsorption and desorption data. When ashed in air, the BET surface area of WRHA increases with ashing temperature firstly, from 60.5 m^2 g^{-1} at 300 °C to 98.7 m^2 g^{-1} at 450 °C due to the decomposition of organic compounds in rice hull. Thereafter, however, the surface area starts to decrease because of the closure of pores induced by the surface melting of oxides (e.g., SiO_2, K_2O) and formation of crystalline crystobalite. The BET surface area of WRHA that ashed at 600 and 750 °C are only 19.0 and 5.1 m^2 g^{-1}, respectively. On the other hand, because the presence of nitrogen will retain the carbon and retard the surface melting and formation of crystobalite, the closure of pores will be hindered when ashed in nitrogen. As a result, the BET surface area of BRHA increases with ashing temperature, from 3.8 m^2 g^{-1} at 300 °C to more than 300 m^2 g^{-1} at 600 and 750 °C.

Figure 7 and Table 2 show the derived pore volumes and pore size distributions of RHA samples. All samples except A750 present similar pore size distributions with maximum micropore volume at 1.4–1.5 nm and maximum mesopore volume at 3.7 nm. It is attributed to the hierarchical distributions of silica framework in rice hull, where loosely cross-linked silica forms mesopores and densely linked produces micropores. The pore volumes of RHA vary with ashing temperatures and atmospheres. When ashed in air, the micropore volume of WRHA increases with ashing temperature firstly, and reach a maximum at

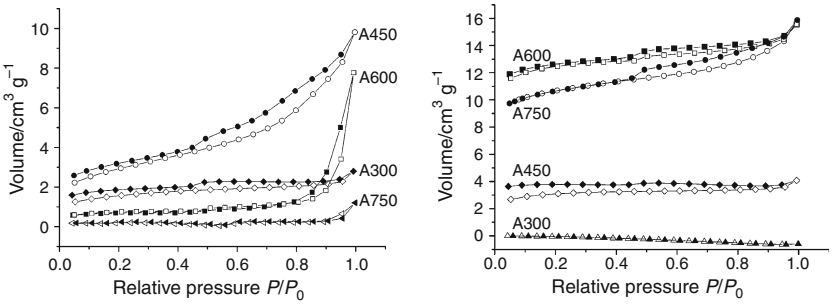

Fig. 6 Nitrogen adsorption (*hollow patterned lines*) and desorption curves (*solid patterned lines*) of RHA samples

Table 2 Nitrogen adsorption and desorption analyses of RHA samples

Samples	BET surface area/m^2 g^{-1}	Total pore volume/ cm^3 g^{-1}	Micropore volume/ cm^3 g^{-1}	Mesopore volume/ cm^3 g^{-1}	Mesopore fraction/%	Average pore size/nm
A300	60.5	0.0541	0.0242	0.0299	55.27	3.01
A450	98.7	0.1675	0.0394	0.1281	76.48	5.72
A600	19.0	0.1029	0.0092	0.0997	91.55	21.07
A750	5.7	0.0218	0.0028	0.0190	87.16	11.35
N300	3.8	–	–	–	–	–
N450	97.0	0.0559	0.0411	0.0148	26.48	2.30
N600	347.7	0.2418	0.1676	0.0742	30.69	2.44
N750	309.0	0.2645	0.1467	0.1178	44.54	2.88

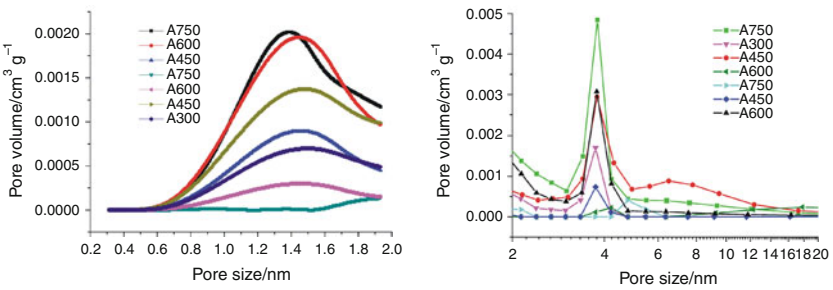

Fig. 7 Pore size distributions of RHA samples: *left*: micropore, *right*: mesopore

450 °C due to the enhanced decomposition of organic substances. Subsequently, however, it starts to decline sharply because of the melting of oxides and closure of micropores. The mesopore volume of WRHA exhibits similar variations, showing a firstly increase and subsequent decrease. The decreasing speed of mesopore volume is much lower than that of micropore volume, attributed to the fact that micropores will be melted to mesopores firstly, and mesopores was melted to macropores thereafter. As a result, the micropore volume of RHA declines sharply from 0.0394 cm^3 g^{-1} at 450 °C to 0.0092 cm^3 g^{-1} at 600 °C, while the mesopore volume decreases slightly from 0.1281 to 0.0997 cm^3 g^{-1}. The significantly decreasing of micropore volume increases the average pore size of RHA, from 5.72 nm at 450 °C to 21.07 nm at 600 °C. When the temperature was further increased to 750 °C, the micropores are almost completely closed and massive mesopores were melted to macropores. Therefore, the total pore volume, micro pore volume, and mesopore volume of A750 are all much lower than that of A300, A450, and A600.

Nitrogen atmosphere will retain the carbon during the decomposition of RHA, and therefore, retard the melting of oxides and closure of micro- and meso-pores. Consequently, the micropore volume, mesopore volume, and total pore volume of BRHA increase with ashing temperature from 300 to 750 °C without descents. The micropore volume of RHA increases from 0.0411 cm^3 g^{-1} at 450 °C to more than 0.14 cm^3 g^{-1} at 600 and 750 °C, while the mesopore volume increases from 0.0148 cm^3 g^{-1} at 450 °C to 0.1178 cm^3 g^{-1} at 750 °C. The increasing rate of mesopore volume is higher than that of micropore

volume, result in increasing of mesopore fraction and average pore size with ashing temperature, from 26.46% and 2.30 nm at 450 °C to 44.54% and 2.88 nm at 750 °C. Due to the preservation of carbon, the micropore volume, BET surface area of BRHA are much higher than that of WRHA.

Conclusions

In summary, we have systematically studied the effects of ashing temperature and atmosphere on the physico-chemical and pore characteristics of rice hull. All RHA samples are porous materials with amorphous nature. The FT-IR spectra indicate that WRHA present more polar groups on the surface than that of BRHA. Higher ashing temperature will enhance the thermal decomposition of rice hull, and nitrogen atmosphere will hinder the thermal decomposition and retain the carbon in rice hull. Therefore, BRHA exhibits higher carbon content, BET surface area, micropore volume, and lower silica content and meso pore fraction than that of WRHA. The surface area and pore volumes of BRHA increase with temperature, while that of WRHA increase with temperature firstly and decline subsequently. This study will provide essential information for choosing a suitable thermal treatment of rice hull for a given adsorbate.

Acknowledgements This research is supported by the "Fundamental Research Funds for the Central Universities", the ministry of Education, People's Republic of China.

References

1. Production yearbook. Basic Data Unit Statistics Division, Food and Agricultural Organization of the United Nations. Rome: Food and Agriculture Organization; 1993.
2. Salas A, Delvasto S, Mejia De Gutierrez R, Lange D. Comparison of two processes for treating rice husk ash for use in high performance concrete. Cem Concr Res. 2009;39:773–8.
3. Daud NK, Hameed BH. Decolorization of acid red 1 by Fenton-like process using rice husk ash-based catalyst. J Hazard Mater. 2010;176:938–44.
4. Bhagiyalakshmi M, Anuradha R, Palanichamy M, Jang HT. Dexterous template-free synthesis of ferrisilicate with MFI morphology using rice husk ash. J Non-Cryst Solids. 2010;356:1204–9.
5. Deiana C, Granados D, Venturini R, Amaya A, Sergio M, Tancredi N. Activated carbons obtained from rice husk: influence of leaching on textural parameters. Ind Eng Chem Res. 2008;47:4754–7.
6. Kalderis D, Bethanis S, Paraskeva P, Diamadopoulos E. Production of activated carbon from bagasse and rice husk by a single-stage chemical activation method at low retention times. Bioresour Technol. 2008;99:6809–16.
7. Guo Y, Yang S, Fu W, Qi J, Li R, Wang Z, Xu H. Adsorption of malachite green on micro- and mesoporous rice husk-based active carbon. Dyes Pigments. 2003;66:123–8.
8. Bondioli F, Barbieri L, Ferrari AM, Manfredini T. Characterization of rice husk ash and its recycling as quartz substitute for the production of ceramic glazes. J Am Ceram Soc. 2010;93:121–6.
9. Sun L, Gong K. Silicon-based materials from rice husks and their applications. Ind Eng Chem Res. 2001;40:5861–77.
10. Yusof AM, Nizam NA, Rashid NAA. Hydrothermal conversion of rice husk ash to faujasite-types and NaA-type of zeolites. J Porous Mater. 2010;17:39–47.
11. Katsuki H, Komarneni S. Synthesis of Na-A and/or Na-X zeolite/porous carbon composites from carbonized rice husk. J Solid State Chem. 2009;182:1749–53.
12. Chen XG, Lv SS, Ye Y, Cheng JP, Yin SH. Preparation and characterization of rice husk ferrite composites. Chin Chem Lett. 2010;21:122–6.
13. Lv SS, Chen XG, Ye Y, Yin SH, Cheng JP, Xia MS. Rice hull/$MnFe_2O_4$ composite: preparation, characterization and its rapid microwave-assisted COD removal for organic wastewater. J Hazard Mater. 2009;171:634–9.
14. Ye H, Zhu Q, Du D. Adsorptive removal of Cd(II) from aqueous solution using natural and modified rice husk. Bioresour Technol. 2010;101:5175–9.
15. Sud D, Mahajan G, Kaur MP. Agricultural waste material as potential adsorbent for sequestering heavy metal ions from aqueous solutions—a review. Bioresour Technol. 2008;99:6017–27.
16. Feng Q, Lin Q, Gong F, Sugita S, Shoya M. Adsorption of lead and mercury by rice husk ash. J Colloid Interface Sci. 2004;163:1254–64.
17. El-Halwany MM. Study of adsorption isotherms and kinetic models for methylene blue adsorption on activated carbon developed from Egyptian rice hull (Part II). Desalination. 2010;250:208–13, 492.
18. Lakshmi UR, Srivastava VC, Mall ID, Lataye DH. Rice husk ash as an effective adsorbent: evaluation of adsorptive characteristics for Indigo Carmine dye. J Environ Manag. 2009;90:710–20.
19. Mohamed MM. Acid dye removal: comparison of surfactant-modified mesoporous FSM-16 with activated carbon derived from rice husk. J Colloid Interface Sci. 2004;21:667–72.
20. Ng SL, Seng CE, Lim PE. Bioregeneration of activated carbon and activated rice husk loaded with phenolic compounds: kinetic modeling. Chemosphere. 2010;78:510–6.
21. Foo KY, Hameed BH. Utilization of rice husk ash as novel adsorbent: a judicious recycling of the colloidal agricultural waste. Adv Colloid Interface. 2009;152:39–47.
22. Lataye DH, Mishra IM, Mall ID. Adsorption of alpha-picoline onto rice husk ash and granular activated carbon from aqueous solution: equilibrium and thermodynamic study. Chem Eng J. 2009;147:139–49.
23. Srivastava VC, Mall ID, Mishra IM. Characterization of mesoporous rice husk ash (RHA) and adsorption kinetics of metal ions from aqueous solution onto RHA. J Hazard Mater. 2006;134:257–67.
24. Simoes RD, Rodriguez-Perez MA, de Saja JA, Constantino CJL. Thermomechanical characterization of PVDF and P (VDF-TrFE) blends containing corn starch and natural rubber. J Therm Anal Calorim. 2010;99:621–9.
25. King A, Kaletun CCG. Retrogradation characteristics of high hydrostatic pressure processed corn and wheat starch. J Therm Anal Calorim. 2009;98:83–9.
26. Mohamed MM, Zidan FI, Thabet M. Synthesis of ZSM-5 zeolite from rice husk ash: characterization and implications for photocatalytic degradation catalysts. Microporous Mesoporous Mater. 2008;108:193–203.

27. Sookkumnerd C, Ito N, Kito K. Financial viabilities of husk-fueled steam engines as an energy-saving technology in Thai rice mills. Appl Energy. 2005;82:64–80.
28. Rodriguez-Reinoso F, Molina-Sabio M. Activated carbons from lignocellulosic materials by chemical and/or physical activation: an overview. Carbon. 1992;30:1111–8.
29. Sharma A, Rao TR. Kinetics of pyrolysis of rice husk. Bioresour Technol. 1999;406:1–7.
30. Vlaev LT, Markovska IG, Lyubchev LA. Non-isothermal kinetics of pyrolysis of rice husk. Thermochim Acta. 2003;35:213–20.
31. Chiang W, Fang H, Wu C, Chang C, Chang Y, Shie J. Pyrolysis kinetics of rice husk in different oxygen concentrations. J Environ Eng. 2008;134:316–25.
32. Markovska IG, Lyubchev LA. A study on the thermal destruction of rice husk in air and nitrogen atmosphere. J Therm Anal Calorim. 2007;89:809–14.
33. Abe I, Hayashi K, Hirashima T, Kitagawa M, Kuroki N. Relation of adsorptive property of hydrophobic porous adsorbents and their surface area and pore volume. J Colloid Interface Sci. 1983;93:572–3.
34. Koretsky CM, Sverjensky DA, Sahai N. A model of surface site types on oxide and silicate minerals based on crystal chemistry; implications for site types and densities, multi-site adsorption, surface infrared spectroscopy, and dissolution kinetics. Am J Sci. 1998;298:349.
35. Nakbanpote W, Thiravetyan P, Kalambaheti C. Preconcentration of gold by rice husk ash. Miner Eng. 2000;13:391–400.
36. Chandrasekhar S, Pramada PN. Rice husk ash as an adsorbent for methylene blue—effect of ashing temperature. Adsorption. 2006; 12:27–43.
37. Ho YS, Chiang CC, Hsu YC. Sorption kinetics for dye removal from aqueous solution using activated clay. Sep Sci Technol. 2001;36:2473–88.
38. Patel M, Karera A, Prasanna P. Effect of thermal and chemical treatments on carbon and silica contents in rice husk. J Mater Sci. 1987;22:2457–64.
39. Chandrasekhar S, Satyanarayana KG, Pramada PN, Raghavan P, Gupta TN. Review processing, properties and applications of reactive silica from rice husk—an overview. J Mater Sci. 2003; 38:3159–68.
40. Gregg SJ, Sing KSW. Adsorption, surface area and porosity. 2nd ed. London: Academic Press; 1982.
41. Tanev PT, Vlaev LT. An attempt at a more precise evaluation of the approach to mesopore size distribution calculations depending on the degree of pore blocking. J Colloid Interface Sci. 1993; 160:110–6.